Tetrahedral Ordering in Water: Raman Profiles and Their Temperature Dependence

ARTICLE *in* THE JOURNAL OF PHYSICAL CHEMISTRY A · NOVEMBER 2009

Impact Factor: 2.69 · DOI: 10.1021/jp9052083 · Source: PubMed

4 AUTHORS, INCLUDING:

Noelia Faginas Lago
Università degli Studi di Perugia
48 PUBLICATIONS **252** CITATIONS
SEE PROFILE

Margarita Albertí Wirsing
University of Barcelona
92 PUBLICATIONS **941** CITATIONS
SEE PROFILE

A. Laganà
Università degli Studi di Perugia
162 PUBLICATIONS **2,220** CITATIONS
SEE PROFILE

Tetrahedral Ordering in Water: Raman Profiles and Their Temperature Dependence†

M. Paolantoni,*,‡ N. Faginas Lago,‡ M. Albertí,§ and A. Laganà‡

Dipartimento di Chimica, Università di Perugia, Via Elce di Sotto, 8, I-06123 Perugia, Italy, and IQTCUB, Departament de Química Física, Universitat de Barcelona, Barcelona, Spain

Received: June 3, 2009; Revised Manuscript Received: October 22, 2009

The supramolecular organization of liquid water is discussed in connection with both the spectral profile of the OH stretching Raman signal measured in pure water and the distribution of tetrahedral order computed by molecular dynamics simulations. Both curves show common features and a similar temperature dependence never pointed out before. Energetic information extracted from the Raman profiles using a recently proposed integration method is also discussed. Overall results confirm that thermally induced structural variations of water in the interval of temperature ranging from 10 to 75 C involve a change of the local tetrahedral order associated with a redistribution energy of 1.6−1.7 kcal/mol.

I. Introduction

The understanding of the intermolecular structure and of the energetic of the coordination shell in liquid water is a challenging problem. Usually they are described in terms of an extended hydrogen bonding network in which many water molecules form four hydrogen bonds (H-bonds) with the nearest neighbors.[1−3] This means that a large fraction of the molecules in the liquid phase are considered to be engaged in 4-fold coordinated local structures of tetrahedral type like in solid ice ("icelike" species). The formation of such an open tetrahedral network at low temperature agrees with the occurrence of a density maximum at 4 C[4,5] and is in line with the hypothesis of the existence of two liquid phases in the supercooled region.[6] The formation of a tetrahedral network for bulk water can also be inferred from an analysis of the X-ray absorption spectra[7] and is supported by molecular mynamics (MD) simulations.[8] Moreover, the distribution of the electric field E ($p(E)$)[8,9] acting on the OH bond calculated using the SPC/E force field[10] reproduces the shape of the Raman stretching band of uncoupled OHs (i.e., HOD diluted in D_2O), which is consistent with a local tetrahedral clustering of water molecules.

A different way of picturing this situation is the one proposed by Wernet et al.[11] who interpret X-ray Raman and X-ray absorption spectra in terms of water molecules forming only two strong H-bonds acting like H-bond donors and acceptors. From this perspective, supported by density functional theory calculations, H-bonded chains and rings are believed to be the dominant structures with a fraction of tetrahedrally coordinated species playing a secondary role in the liquid phase. Recently, Tokushima et al.[12] from X-ray emission spectra argued that at room temperature the dominant structures for water are strongly distorted H-bond and tetrahedral species with a ratio of 2:1.

As to the evaluation of the energy change involved in thermal rearrangements of water, Smith et al.[7] associated the main features of the X-ray spectra to the existence of two classes of molecular structures, icelike and broken-donor (in the latter class water molecules participate in broken or distorted H-bonds). On this basis they estimated that the difference in the average energy of the two classes amounts to 1.5 ± 0.5 kcal/mol. This value agrees with the H-bonding energy (1.4 ± 0.2 kcal/mol) derived by a van't Hoff analysis of the temperature dependence of the Raman band of water obtained from a novel integration method of the spectra.[7] On the other hand, the van't Hoff analysis of OH Raman profiles based on a classical Gaussian bands deconvolution, originally proposed by Walrafen,[2] leads to values of the OH binding energy ranging from 2.5 to 2.8 kcal/mol (these values are commonly considered as reference data for the H-bond breaking in water[13−16]).

From this point of view MD calculations represent an appropriate computational way of determining relevant properties of liquid water. In particular, from MD calculations one can determine $f(q,T)$, the distribution of the orientational parameter q, which gives an estimate of the local tetrahedral organization at a given temperature T.[17−19] This is what is discussed in the present paper in which the measured isotropic Raman profile of pure water is rationalized in terms of the $f(q,T)$ distribution and energetic information is obtained from its temperature dependence.

Accordingly, the paper is organized as follows: in Section II experimental and computational methods are illustrated; in Section III related results are discussed; and in Section IV some conclusions are drawn.

II. Experimental and Computational Methods

Raman spectra of pure water in the OH stretching region (2800−3800 cm^{-1}) were obtained in the 10−75 C temperature range. Doubly distilled and deionized water was prepared in our laboratory. Raman spectra were recorded using an ISA Jobin-Yvon model U1000 double monochromator (1 m focal length holographic gratings) and photon counting detection. The 514.5 nm line of an argon ion laser (Coherent model Innova 90) in single-line excitation mode was employed as a light source. The power focused on the samples was always less than 600 mW. The detection device was a thermoelectrically cooled photomultiplier (Hamamatsu model 943XX) computer controlled by the ISA Jobin−Yvon SpectraMax package through a photon counting chain and an acquisition board system. The spectra were recorded with vertical−vertical (VV) and horizontal−vertical (HV) polarization scattering geometries using standard polarization optics (Melles−Griot). The system was standardized by measuring the

† Part of the "Vincenzo Aquilanti Festschrift".
* To whom correspondence should be addressed.
‡ Università di Perugia.
§ Universitat de Barcelona.

10.1021/jp9052083
Published on Web 11/06/2009

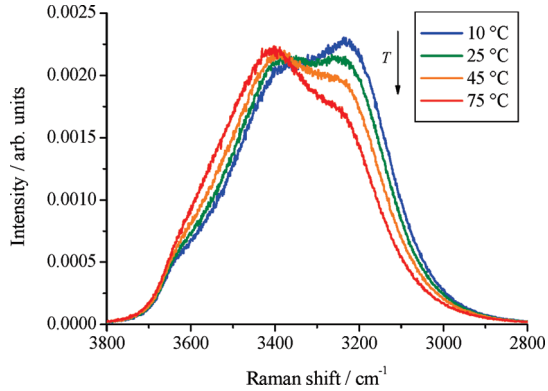

Figure 1. Fully corrected isotropic profiles (isosbestic at ca. 3355 cm^{-1}) determined at different temperature values. The arrow indicates the direction along which the temperature increases.

depolarization ratios of symmetric and antisymmetric modes of liquid CCl_4. Isotropic profiles I_{ISO} were obtained from VV and HV spectra (I_{VV} and I_{HV}, respectively) by the usual formula ($I_{ISO} = I_{VV} - (4/3)I_{HV}$) recording sequences of HV, VV, and HV spectra in order to account for the long-time drift of the experimental setup. During each acquisition, the temperature was controlled by circulating water from a Haake F6 ultrathermostat (precision of 0.1 C).

Energy properties were calculated from band profiles using the already mentioned novel integration method in which the contribution of two classes of OH oscillators are estimated by integrating the spectral distribution for frequencies (ν) smaller and larger than the isosbestic frequency (ν_{IB}),[7,9,20] respectively, rather than using the more conventional method of deconvoluting the signal in subcomponents.[2,21,22] In this approach, a van't Hoff plot is constructed by considering the temperature dependence of the ratio of the area of the spectrum at $\nu < \nu_{IB}$ (associated with icelike configurations) and the area at $\nu > \nu_{IB}$ (associated with distorted or broken H-bonds).[7,9,20]

Classical molecular dynamics simulations have been performed using the DL_POLY suite of codes.[23] Each run was carried out for a canonical ensemble (NVT) of water molecules in a cubic box with periodic boundary conditions. The temperature was varied from 5 to 100 C and kept under control using the Berendsen method. The volumes were set to reproduce the experimental values of the corresponding water density[24] at the chosen temperature. The SHAKE method was used to handle the constraints and the Verlet algorithm was employed to integrate the equations of motion. The integration time step was chosen to be 2 fs for trajectories integrated for 1 ns. All simulations, were started from the same initial set of coordinate values and were performed under exactly the same conditions with the exception of temperature and volume. The calculations were performed using the SPC/E potential.[10] Short-range interactions were cut at one-half on the box length while long-range electrostatic interactions were evaluated by means of the Ewald summation.[25]

III. Results and Discussion

Raman Experiments. Representative isotropic OH stretching Raman profiles of neat water, $I^*_{ISO}(\nu,T)$, obtained at different values of the temperature T are plotted in Figure 1 in the ν range going from 3800 to 2800 cm^{-1}, after correcting the measured intensity $I_{ISO}(\nu,T)$ for the intrinsic frequency dependence of the Raman scattering process.[26] For this purpose the following expression

$$I^*_{ISO}(\nu,T) = \nu[1 - \exp(-h\nu/kT)](\nu_L - \nu)^{-3} I_{ISO}(\nu,T) \quad (1)$$

was used in which h is the Planck constant, k is the Boltzmann constant, ν_L is the frequency of the incident radiation, $(\nu_L - \nu)^{-3}$ is a factor accounting for the frequency dependence of the efficiency of the scattering process in the photon-counting detection mode[27] and $[1 - \exp(-h\nu/kT)]$ is the population factor. The reason for using $I^*_{ISO}(\nu,T)$ rather than the measured intensity $I_{ISO}(\nu,T)$ lies in the fact that the former better represents the vibrational density of the OH states.

The $I^*_{ISO}(\nu,T)$ profiles clearly show two main spectral features centered at 3250 and 3400 cm^{-1}, respectively. The lower frequency feature is usually associated with a collective symmetric stretching mode in which the OH oscillators of the nearest molecules undergo an all in-phase oscillation[2,21,28-30] in local tetrahedral arrangements of fully coordinated H-bonded water molecules with unstrained H-bonds. The higher frequency feature is still mainly associated with H-bonded water molecules, yet having reduced phase correlations among nearest OH groups.[21,30] From a structural point of view they are often called as open and closed, respectively.[31] The Raman profiles show also a much higher frequency shoulder centered at ca. 3600 cm^{-1} usually associated with the vibration of the OH groups not involved, as proton-donors, in the formation of H-bonds (i.e., free OH groups).[13,21] These oscillators are weakly stabilized by H-bond interactions and may be considered as transient species.[32]

The role played by the intermolecular vibrational coupling in determining the importance of the 3250 cm^{-1} component is emphasized by the fact that its intensity decreases with isotopic dilution.[26,28] A theoretical study[33] suggests that the intermolecular vibrational coupling in neat water essentially occurs through a transition dipole-transition dipole mechanism fostering a resonant delocalization of vibrational energy over coupled water molecules (in a time-domain picture this corresponds to an ultrafast transfer of vibrational energy).[33,34] As a matter of fact the VV Raman profile has been recently calculated by Auer and Skinner[35] including both inter- and intramolecular coupling effects and it is demonstrated that the weighted frequency distribution of pure water exhibits an additional 3250 cm^{-1} component due to the intermolecular coupling. The authors claim that even if the coupling between the OH oscillators is relatively modest, vibrations are largely delocalized and involve several molecules. For this reason, the Raman spectrum of water shows the low-frequency component specifically related to molecular configurations bearing favorable vibrational coupling that strongly depend on intermolecular distances and angles. Obviously, this does not imply per se the existence of tetrahedral ordering (for instance, intermolecular delocalization of vibrational energy is effective also in alcohols for which linear H-bonded structures dominate[36,37]).

The plots of Figure 1 show that the spectral structure deforms and shifts to higher frequencies as the temperature increases. In particular, the low-frequency maximum rapidly turns into a shoulder while the higher frequency one becomes more pronounced and ends up by masking the 3600 cm^{-1} structure almost completely. The plotted profiles were rescaled by taking into account the weak temperature dependence of the VV Raman intensity reported by Hare and Sorensen.[38] Rescaled spectra show an isosbestic point at ca. 3355 ± 5 cm^{-1} in reasonable agreement with the findings of Walrafen et al. (isosbestic at 3370 cm^{-1}).[13]

The temperature dependence of Raman spectra, which is directly related to the H-bond redistribution within the system,

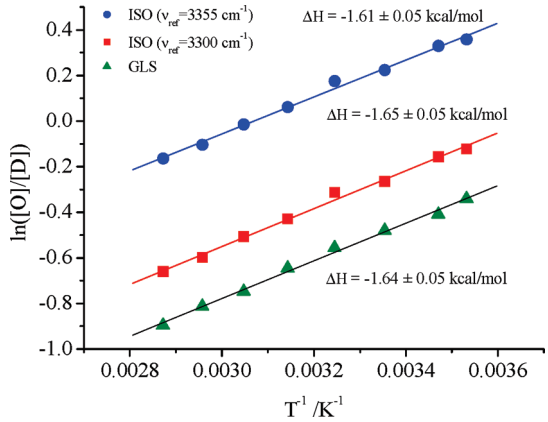

Figure 2. van't Hoff plot of the ratio between ordered (O) and disordered (D) species evaluated using the new integration method on Raman isotropic profiles (circles and squares) with different reference frequencies. The corresponding plot obtained by the GLS stripping procedure is also shown (triangles).

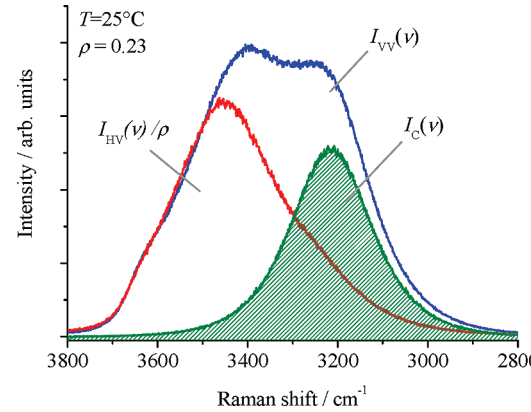

Figure 3. Sketch of the GLS "stripping procedure" of OH Raman bands. The $I_C(\nu)$ curve represents the collective component defined in eq 2.

was used to evaluate the amount of energy associated with the thermal rearrangement of water. Usually, as already mentioned, these spectral changes are rationalized by assuming the existence of a pseudochemical equilibrium between H-bonded and non-H-bonded ensembles, both in continuous and multistates models.[2,7,9,16] Because of the origin of the two main features of the Raman profiles discussed above, the observed variations can be largely attributed to the thermally induced disordering effect on icelike structures and the involved pseudochemical equilibrium can be assumed to refer to ordered (O) and disordered (D) water environments (in this respect only water molecules participating in highly symmetric tetrahedral structures are expected to contribute to the O population). In our van't Hoff treatment, we first apply the already described integration procedure[7,9,20] to the corrected isotropic Raman spectra of Figure 1 using the isosbestic point $\nu_{IB} = 3355 \pm 5$ cm^{-1} as reference frequency ($\nu_{REF} = \nu_{IB}$) in order to separate the two subensembles. Using this ν_{REF} value a $\Delta H = 1.61 \pm 0.05$ kcal/mol was obtained for the O↔D equilibrium (see upper curve of Figure 2). The use of VV Raman spectra and of the related isosbestic point ($\nu_{REF} = \nu_{IB} = 3390 \pm 5$ cm^{-1}) led to a slightly lower rearrangement energy value ($\Delta H = 1.36 \pm 0.07$ kcal/mol) in agreement with the result obtained when all the polarized components of the scattered light (i.e., VV + VH) were detected.[7] It was also checked that the spectral corrections of eq 1 scarcely affect the estimated energies.

The uncoupled OH stretching of HOD species diluted in D_2O shows instead the isosbestic at higher frequencies ($\nu_{IB} = 3480$ cm^{-1}) and gives a somewhat larger rearrangement energy value ($\Delta H = 2.0 \pm 0.1$ kcal/mol).[9] Overall results indicate that Raman data when analyzed with the proposed integration method provide energy values ranging from 1.4 to 2.0 kcal/mol for both coupled and uncoupled OH modes with these values being weakly dependent on the polarization configuration and on the correction considered (eq 1). These values agree with the one inferred in ref 7 by modeling X-ray data (1.5 ± 0.5 kcal/mol). However as already remarked in ref 9 within the framework of a continuous description of H-bonding interactions, the isosbestic frequency is only an arbitrary bisecting point. Still, when the measured profiles reproduce the density of states, ν_{IB} represents the frequency of those OHs with a configuration energy similar to the average energy of the ensemble and, therefore, it can be considered a useful reference frequency.[9] Yet the ν_{IB} in the isotropic Raman spectra of neat water is substantially red shifted when compared with the diluted sample, consistently with the relative increase of Raman cross section at lower frequencies. Thus, in this case ν_{IB} may be not mutually representative when different distributions are compared. With reference to the coupled Raman spectra it seems reasonable to take a value of ν_{REF} equal to 3300 cm^{-1} (in the between of the two main components) in order to separate O from D species. The resulting ΔH is equal to 1.65 ± 0.05 kcal/mol (see intermediate curve of Figure 2). This fact points out that the dependence of the resulting ΔH on the value of the bisecting ν_{REF} is weak as long as ν_{REF} is far enough from the edges of the distribution. Notably, $\nu_{REF} = 3300$ cm^{-1} is located in the extreme low-frequency side of the uncoupled spectrum[9] ($\nu_{IB} = 3480$ cm^{-1}). The similarity of the deduced ΔH for coupled and uncoupled profiles can be explained considering that in pure water the intermolecular coupling selectively shifts to $\nu < 3300$ cm^{-1} the vibrational modes of ordered icelike species and that the reduction of these tetrahedral environments is also responsible of the temperature dependence for the uncoupled spectrum at $\nu < 3480$ cm^{-1}.

In order to isolate the icelike component from Raman data the popular GLS spectral decomposition method introduced by Green, Lacey, and Sceats[28] that formulates $I_{VV}(\nu,T)$ as a sum of a rescaled $I_{HV}(\nu,T)$ and the collective icelike contribution $I_C(\nu,T)$ has been used (see Figure 3). The GLS method assumes that the HV Raman spectrum is a rescaled version of the VV one though without the inclusion of the strongly polarized in-phase mode component. $I_C(\nu,T)$ is then evaluated from the equation

$$I_C(\nu, T) = I_{VV}(\nu, T) - (I_{HV}(\nu, T)/\rho) \qquad (2)$$

in which $I_{VH}(\nu,T)/\rho$ is the rescaled HV spectrum with $\rho = 0.23$ being the depolarization ratio of the high frequency portion of the Raman spectrum (that is in practice temperature independent).[28] This means that the relative intensity of the collective component $C(T)$, that can be obtained as the normalized area

$$C(T) = \int I_C(\nu, T)\mathrm{d}\nu / \int I_{VV}(\nu, T)d\nu \qquad (3)$$

is an estimate of the fraction of ordered water species. Out of this we can build the corresponding van't Hoff plot of the $C(T)/(1 - C(T))$ ratio (see the lower curve in Figure 2) that leads to $\Delta H = 1.64 \pm 0.05$ kcal/mol in satisfactory agreement with the values previously quoted. Despite the popularity of the GLS

method to quantify the extent of tetrahedral order in aqueous systems,[22,28,39] to our knowledge, its use for the evaluation of the energy changes in water reorganization has never been pointed out before.

From this point of view the integration method described above represents a simple and convenient tool to analyze the thermal behavior of Raman profiles and is consistent with the "stripping approach" of GLS employed for the separation of the collective icelike component.[28] This means also that the $\Delta H = 1.6-1.7$ kcal/mol value can be accepted as a good estimate of the average energy necessary to change liquid water local configurations from icelike to more disordered environments.[7]

Interestingly, the value of the H-bonding energy in normal liquid alcohols is around 6 kcal/mol[40] which recalls the H-bond breaking energy evaluated considering the sublimation enthalpy of water (ca. 5.7 kcal/mol).[1,3] In liquid alkanols, a standard van't Hoff treatment of Raman profiles,[41] which show a sharp high frequency signal ($\nu > 3600$ cm^{-1}) due to free OHs, leads to a H-bond enthalpy of 5.3 ± 0.1 kcal/mol. This suggests that the strength of a single H-bond in water and alcohols is similar and that for these latter the Raman data provide an estimate of the H-bond breaking energy value. On the other hand, the small value of ΔH determined in liquid water essentially refers to the distortion of ordered configurations (i.e., to the O → D process) with only minor contributions arising from the H-bond breaking process. Furthermore, depolarized Rayleigh scattering (DRS) experiments in water evidence the presence of a relaxation process at picosecond time scales (often identified as the H-bond lifetime[42−44]) with a typical activation energy (E_A) of 2.6−2.9 kcal/mol. This value agrees with the enthalpy variation obtained from conventional deconvolution methods of OH Raman bands[2,13,15,16,22] and is somewhat larger than the above-mentioned ΔH value (1.6−1.7 kcal/mol). This situation may be understood in terms of the fact that (i) the DRS relaxation is due to a structural rearrangement involving also partial H-bond breakings which makes $E_A > \Delta H$ and (ii) classical deconvolutions define a high frequency OH subensemble that involves a significant contribution from very weak or broken H-bonds.

Molecular Dynamics Calculations. To carry out MD calculations, the intermolecular interaction has been described using the SPC/E model[10] in which water molecules interact through a pairwise-additive sum of atom (i)-atom (j) potentials $V(r_{ij})$. This model is made of a first (see eq 4) van der Waals term formulated as 12-6 Lennard-Jones potential $V_{LJ}(r_{ij})$ and a second (see eq 4) electrostatic term $V_{el}(r_{ij})$ between partial charges q_i and q_j

$$V(r_{ij}) = 4\varepsilon_{ij}\left[\left(\frac{\sigma_{ij}}{r_{ij}}\right)^{12} - \left(\frac{\sigma_{ij}}{r_{ij}}\right)^{6}\right] + \frac{q_i q_j}{4\pi\varepsilon_0 r_{ij}} \qquad (4)$$

where r_{ij} is the intermolecular atom−atom distance. The $V_{LJ}(r_{ij})$ only accounts for oxygen−oxygen interactions ($\varepsilon_{OO} = 0.1553$ kcal/mol and $\sigma_{OO} = 3.165$ Å) while a three point charge molecular distribution is considered for the $V_{el}(r)$ term with $q_O = -0.8476$ au and $q_H = +0.4238$ au. Only $V_{el}(r_{ij})$ determines intermolecular directional effects.

As already mentioned, ordering information can be obtained from the orientation parameter q that was initially introduced by Chau and Hardwick.[17] A rescaled formulation of q was provided by Errington and Debenedetti.[18] For the generic water molecule i the q parameter may be defined as follows[18,19,45−47]

$$q_i = 1 - \frac{3}{8}\sum_{j=1}^{3}\sum_{k=j+1}^{4}\left(\cos\psi_{ijk} + \frac{1}{3}\right)^2 \qquad (5)$$

where Ψ_{ijk} is the angle formed between the oxygen atom of the central water molecule i and the oxygen atoms of its neighboring water molecules j and k. The sum of eq 5 is over distinct pairs of the four closest neighbors of molecule i (i.e., there are six possible O−O−O angles per molecule). For an ideal gas for which a local order cannot be defined, q vanishes whereas in a perfect tetrahedral arrangement $q = 1$. The outcome of the MD calculations is rationalized in terms of plots of the resulting $f(q,T)$ distributions (normalized to a unit area) at different temperatures. We note that $f(q,T)$ distributions obtained in MD calculations using different water potentials show common features when compared at the corresponding melting point or maximum density temperatures.[47−49] As apparent from Figure 4 the plots of $f(q,T)$ taken at different temperatures (which agree with previous results[18]) show strong similarities with the corresponding plots of $I^*_{ISO}(\nu,T)$ given in Figure 1. As a matter of fact, they show two main components located at about $q \sim 0.5$ and $q \sim 0.8$ which slightly shift to lower q values at higher temperatures. Moreover, when the temperature increases the low-q maximum rises at the expenses of the high-q one leading to a quasi-isosbestic point at $q = 0.62$. This suggests that disordered configurations (low-q component) coexist in liquid water with tetrahedral ones (high-q component) at all T values. Moreover, ordering reduces as temperature increases, and tetrahedral icelike configurations are gradually converted into more disordered ones. Notably, as already mentioned, the existence of local tetrahedral ordering seems to be a basic requisite for the formation of lower density domains in water at low T.[4,5,19] This process also involves more cooperative effects.[19]

The capability of water in forming tetrahedral configurations can be modulated by changing either the relative strength of dispersive interactions with respect to Coulombic interactions in the water potential (hybrid models) or the water geometry (bent models) as attempted in the recent past.[50−53] As an example, following a practice of the recent literature one can increase ε_{OO} in eq 4 to reduce the weight of the electrostatic contribution related to H-bond forces. A larger ε_{OO} leads to larger repulsions, weaker H-bonds and more isotropic interactions and makes the systems more similar to a Lennard-Jones liquid.[50−52] The net result of the loss of anisotropy should imply a smoothing of the $f(q,T)$ structure in the related MD outcomes. In Figure 5 the results of the MD calculations performed on a modified potential in which ε_{OO} was increased by a factor 1.5 (this is the hybrid s15 model in the notation of ref 51) are plotted. As expected, the loss of ordering capacity, following the modification of the potential, dramatically lowers the intensity of the high-q peak component. For the same reason at high temperature $f(q,T)$ becomes almost symmetric and unimodal with a maximum at about $q = 0.50$ that corresponds to the distribution typical of a Lennard-Jones molecular system.[18] A further increase of ε_{OO} by a factor 3 (hybrid s30[51]) makes totally symmetric and unimodal also the low temperature distribution. These findings further confirm the rationalization of the SPC/E $f(q,T)$ in terms of a mixture of ordered and disordered local domains and also suggest that the temperature dependence of the $f(q,T)$ distributions increases with the extent of tetrahedral ordering.

To further explore the connections existing between Raman profiles and the $f(q,T)$ distributions, the latter were analyzed

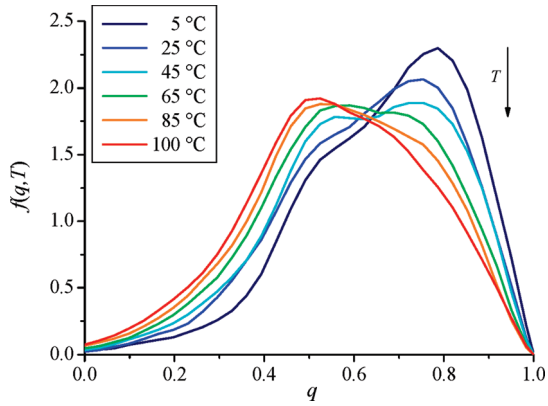

Figure 4. Distribution of the orientational order q calculated at different temperature values obtained using the SPC/E force field. The area under each curve is normalized to unity. The arrow indicates the direction along which the temperature increases.

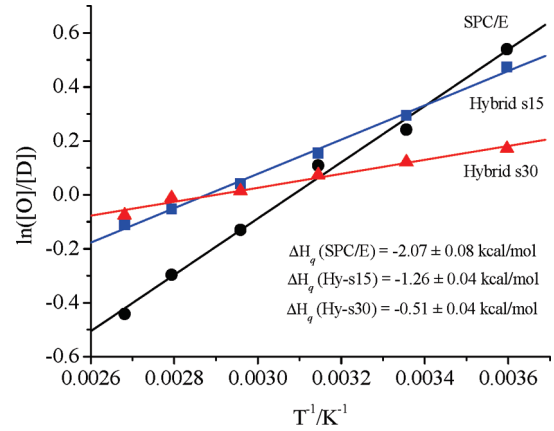

Figure 6. Van't Hoff plot of the ratio between ordered (O) and disordered (D) species evaluated considering the new integration method on $f(q,T)$ distributions obtained for SPC/E (circles), hybrid s15 (squares), and hybrid s30 (triangles) force fields.

using the above-discussed integration procedure. For the $f(q,T)$ distributions calculated using the standard SPC/E parameters (see Figure 4) we took $q = 0.63$, that looks like as an isosbestic point, as the bisecting point q_{REF}. The van't Hoff treatment carried out using this value of q_{REF} led to $\Delta H_q = 2.07 \pm 0.08$ kcal/mol (Figure 6), confirming the validity of the assumption that both Raman and $f(q,T)$ profiles reflect similar thermal transformations involving the switch from tetrahedral to distorted configurations. The resulting ΔH_q also corresponds to the energy difference obtained by Smith et al.[9] when studying the temperature dependence of the electric field distribution ($p(E)$) (1.84 $\pm$ 0.01 kcal/mol). In this respect, OH groups participating in more ordered environments, $q < 0.63$, should experience larger electric fields ($E < -1.5$ V/Å) induced by the surrounding molecules. The van't Hoff analysis of the $f(q,T)$ for the s15 ($q_{REF} = 0.53$) and s30 ($q_{REF} = 0.46$) hybrids led to progressively lower ΔH_q values. In this sense, a Lennard-Jones-like system is characterized by a more uniform energy distribution less affected by temperature variations. Thus, the proposed thermal analysis can be said to be informative of the extent of tetrahedral ordering and in principle could be equally well employed to gain structural insights also in water mixtures and in other aqueous systems.

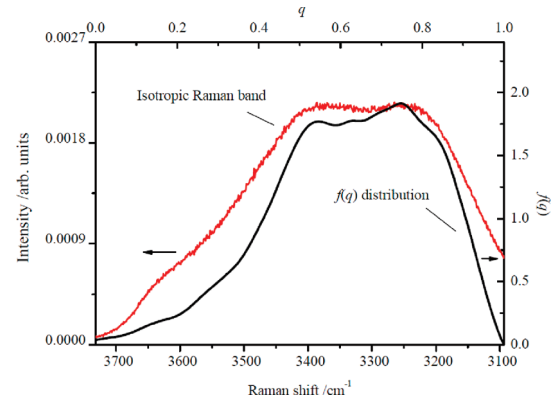

Figure 7. Direct comparison between the isotropic Raman spectrum (25 C) and the distribution of the orientational order $f(q,T)$ (45 C) calculated using the SPC/E force field (see text for details).

IV. Conclusive Comparison and Remarks

A conclusive picture of the investigation reported in the paper is shown in Figure 7 in which a comparison of the isotropic Raman band and the calculated $f(q,T)$ distribution is given. The two profiles show close similarities (also in terms of the temperature dependence) that are pointed out here for the first time and allow a straightforward rationalization of the experimental spectral features in terms of tetrahedral order. In fact, plots of Figure 7 permit a clear association of the low-frequency Raman component at 3235 cm^{-1} with structured environments having $q = 0.78$ and of the high-frequency component at 3400 cm^{-1} with disordered configurations having $q = 0.52$ (these correspondences were obtained comparing spectral distributions taken at the two extreme T values and were used to rescale the

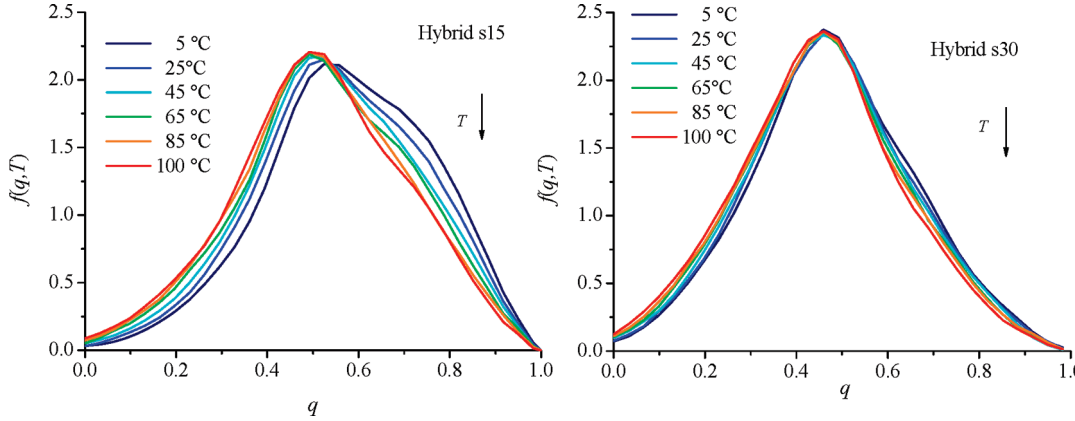

Figure 5. Distribution of the orientational order q calculated at different temperature values obtained using the hybrid potentials (see text for details). The arrow indicates the direction along which the temperature increases. The area under each curve is normalized to unity.

x-axis of Figure 7). It is worth pointing out here that the value $q = 0.52$ characterizes the tetrahedral ordering typical of a Lennard-Jones liquid (see Figure 5) and that the correlation between the Raman spectrum of pure water and the $f(q,T)$ distribution is the consequence of the fact that the intermolecular coupling is particularly efficient for tetrahedral structures whose collective vibrations at lower frequencies show relatively large Raman activities.[38,54] Incidentally, it is worth pointing out here that the best agreement between the $f(q,T)$ and the experimental Raman profile is obtained when the calculated $f(q,T)$ refers to a temperature 20 C higher than the experimental one. This may indicate that as long as the water population fractions are in line with the distribution of the OH Raman spectra[38] the SPC/E force filed leads to an overestimate of the extent of tetrahedral order.

After all, while the distribution $p(E)$ of the electric field E on the OH bond represents a key property which easily explains experimental IR and Raman spectra of vibrationally uncoupled HOD molecules diluted in D_2O,[9,55] our findings indicate that the intermolecular organization described by $f(q,T)$ is the relevant quantity strongly related to the Raman spectral distribution measured in neat water, when the vibrational coupling between OH oscillators occurs.

These findings allowed us to put on a more quantitative basis also the calculation of the energy associated with the thermal rearrangement of water using the recently proposed integration method of band profiles.[7,9,20] The method, starting from fully corrected isotropic profiles ($\nu_{REF} = 3300$ cm^{-1}) led to a ΔH redistribution energy of 1.65 ± 0.05 kcal/mol that nicely agrees with the energy value determined using the GLS procedure[22,28,39] often used to isolate the collective icelike spectral contribution. This correspondence, never explored before, clarifies the physical origin of the detected ΔH value that essentially represents the energy cost necessary to distort ordered tetrahedral configurations in the liquid.

Acknowledgment. M.A. thanks financial support from the Ministerio de Educación y Ciencia (Spain, Project CTQ2007-61109) and from the Ministerio de Ciencia e Innovación (Spain, Mobility Program, Project PR2008-0251). Also thanks are due to the Centre de Supercomputació de Catalunya CESCA-C4 and Fundació Catalana per a la Recerca for the allocated supercomputing time. N.F.L. acknowledges the working group QDYN of the COST CMST European Cooperative Project CHEMGRID (Action D37). Also thanks are due to the COMPCHEM VO for the allocation of computing time.

References and Notes

(1) Eisemberg, D.; Kauzmann, W. *The Structure and Properties of Water*; Clarendon: Oxford 1969.
(2) Walrafen, G, E. Raman and Infrared Spectral Investigations of Water Structure. In *Water: A Comprehensive Treatise*; Franks, F., Ed.; Plenum: New York, 1972; Vol 26; p 151.
(3) Stillinger, F. H. *Science* **1980**, *209*, 451.
(4) Mallamace, F.; Branca, C.; Broccio, M.; Corsaro, C.; Mou, C.-Y.; Chen, S.-H. *Proc. Natl. Acad. Sci. U.S.A.* **2007**, *104*, 18387.
(5) Ludwig, R. *Phys. Chem. Chem. Phys.* **2007**, *8*, 938.
(6) Mishima, O.; Stanley, E. *Nature* **1998**, *396*, 329.
(7) Smith, J. D.; Cappa, C. D.; Wilson, K. R.; Messer, B. M.; Cohen, R. C.; Saykally, R. J. *Science* **2004**, *306*, 851.
(8) Smith, J. D.; Cappa, C. D.; Messer, B. M.; Drisdell, W. S.; Cohen, R. C.; Saykally, R. J. *J. Phys. Chem. B* **2006**, *110*, 20038.
(9) Smith, J. D.; Cappa, C. D.; Wilson, K. R.; Cohen, R. C.; Geissler, P. L.; Saykally, R. J. *Proc. Natl. Acad. Sci. U.S.A.* **2005**, *102*, 14171.
(10) Berendsen, H. J. C.; Grigera, J. R.; Straatsma, T. P. *J. Phys. Chem.* **1987**, *91*, 6269.
(11) Wernet, Ph.; Nordlund, D.; Bergmann, U.; Cavalleri, M.; Odelius, M.; Ogasawara, H.; Näslund, L. Å.; Hirsch, T. K.; Ojamäe, L.; Glatzel, P.; Pattersson, L. G. M.; Nilsson, A. *Science* **2004**, *304*, 995.
(12) Tokushima, T.; Harada, Y.; Takahashi, O.; Senba, Y.; Ohashi, H.; Pattersson, L. G. M.; Nilsson, A.; Shin, S. *Chem. Phys. Lett.* **2008**, *460*, 387.
(13) Walrafen, G. E.; Fisher, M. R.; Hokmabadi, M. S.; Yang, W.-H. *J. Chem. Phys.* **1986**, *85*, 6970.
(14) Agmon, N. *J. Phys. Chem.* **1996**, *100*, 1072.
(15) Carey, D. M.; Korenowski, G. M. *J. Chem. Phys.* **1998**, *108*, 2669.
(16) Walrafen, G. E. *J. Chem. Phys.* **2004**, *120*, 4868.
(17) Chau, P. L.; Hardwick, A. J. *Mol. Phys.* **1998**, *93*, 511.
(18) Errington, J. R.; Debenedetti, P. G. *Nature* **2001**, *409*, 318.
(19) Errington, J. R.; Debenedetti, P. G.; Torquato, S. *Phys. Rew. Lett.* **2002**, *89*, 215503.
(20) Vehring, R.; Schweiger, G. *Appl. Spectrosc.* **1992**, *46*, 25.
(21) Monosmith, W. B.; Walrafen, G. E. *J. Phys. Chem.* **1984**, *81*, 669.
(22) Gallina, M. E.; Sassi, P.; Paolantoni, M.; Morresi, A.; Cataliotti, R. S. *J. Phys. Chem. B* **2006**, *110*, 8856.
(23) The DL_POLY Molecular Simulation Package, http://www.cse.clrc.ac.uk/ccg/software/DL_POLY/index.shtml, accessed November 2, 2009.
(24) Weast, R. C. *CRC Handbook of Chemistry and Physics*, 66th ed.; CRC Press: Boca Raton, FL, 1985.
(25) Allen, M. P.; Tildesley, D. J. *Computer Simulations of Liquids*; Clarendon Press: Oxford, 1990.
(26) Scherer, J. R.; Go, M. K.; Kint, S. *J. Phys. Chem.* **1974**, *78*, 1304.
(27) Kinoshita, S.; Kai, Y.; Yamaguchi, M.; Yagi, T. *Phys. Rew. Lett.* **1995**, *75*, 148.
(28) Green, J. L.; Lacey, A. R.; Sceats, M. G. *J. Phys. Chem.* **1986**, *90*, 3958.
(29) Hare, D. E.; Sorensen, C. M. *J. Chem. Phys.* **1990**, *93*, 25.
(30) Walrafen, G. E.; Chu, Y. C. *J. Phys. Chem.* **1995**, *99*, 11225.
(31) D'Arrigo, G.; Maisano, G.; Mallamace, F.; Migliardo, P.; Wanderlingh, F. *J. Chem. Phys.* **1981**, *75*, 4264.
(32) Eaves, J. D.; Loparo, J. J.; Fecko, C. J.; Roberts, S. T.; Tokmakoff, A.; Geissler, P. L. *Proc. Natl. Acad. Sci. U.S.A.* **2005**, *102*, 13019.
(33) Torii, H. *J. Phys. Chem. A* **2006**, *110*, 9469.
(34) Wuotersen, S.; Bakker, H. J. *Nature* **1999**, *402*, 507.
(35) Auer, B. M.; Skinner, J. L. *J. Chem. Phys.* **2008**, *128*, 224511.
(36) Torii, H. *J. Phys. Chem. A* **1999**, *103*, 2843.
(37) Paolantoni, M.; Sassi, P.; Morresi, A.; Cataliotti, R. S. *J. Raman Spectrosc.* **2006**, *37*, 528.
(38) Hare, D. E.; Sorensen, C. M. *J. Chem. Phys.* **1992**, *96*, 13.
(39) Kitano, H.; Takaha, K.; Gemmei-Ide, M. *Phys. Chem. Chem. Phys.* **2006**, *8*, 1178.
(40) Benson, S. W. *J. Am. Chem. Soc.* **1996**, *118*, 10645.
(41) Palombo, F.; Sassi, P.; Paolantoni, M.; Morresi, A.; Cataliotti, R. S. *J. Phys. Chem. B* **2006**, *110*, 18017.
(42) Teixeira, J.; Luzar, A.; Longeville, S. *J. Phys.: Condens. Matter* **2006**, *18*, S2353.
(43) Paolantoni, M.; Sassi, P.; Morresi, A.; Santini, S. *J. Chem. Phys.* **2007**, *127*, 024504.
(44) Paolantoni, M.; Comez, L.; Fioretto, D.; Gallina, M. E.; Morresi, A.; Sassi, P.; Scarponi, F. *J. Raman Spectrosc.* **2008**, *39*, 238.
(45) Lee, S. L.; Debenedetti, P. G.; Errington, J. R. *J. Chem. Phys.* **2005**, *122*, 204511.
(46) Elola, M. D.; Ladanyi, B. M. *J. Chem. Phys.* **2006**, *125*, 184506.
(47) Jhon, Y.; Tai No, K.; Shik Jhon, M. *J. Phys. Chem. B* **2007**, *111*, 9897.
(48) Conde, M. M.; Vega, C.; Patrykiejew, A. *J. Chem. Phys.* **2008**, *129*, 014702.
(49) Faginas Lago, N.; Huarte Larrañaga, F.; Albertí, M. *Eur. Phys. J. D* **2009**, *55*, 75.
(50) Lynden-Bell, R. M.; Debenedetti, P. G. *J. Phys. Chem. B* **2005**, *109*, 6527.
(51) Lynden-Bell, R. M.; Youngs, T. G. A. *Mol. Simul.* **2006**, *32*, 1025.
(52) Lynden-Bell, R. M.; Head-Gordon, T. *Mol. Phys.* **2006**, *104*, 3593.
(53) Chatterjee, S.; Debenedetti, P. G.; Stillinger, F. H.; Lynden-Bell, R. M. *J. Chem. Phys.* **2008**, *128*, 124511.
(54) Isotropic profiles differ from the actual density of states because of a frequency dependent intensity factor neglected in eq 1. In fact, even neglecting the dependence of the Raman cross section on H-bonding as reasonable for the decoupled HOD mode (Condon approximation[35,55]), it is to be expected that in-phase collective modes leads to a relative Raman enhancement at lower frequencies.[38]
(55) Corcelli, S. A.; Skinner, J. L. *J. Phys. Chem. A* **2005**, *109*, 6154.

JP9052083